Title

Universal Relationshipbetween Limiting Current andElectrochemical Transport Properties in Malonate-Based Polymer Electrolytes

Journal

MACROMOLECULES

ISSN

0024-9297

Authors

Jana, Rounak

Gido, Lily A

Patel, Vivaan

et al.

Publication Date

2026-07-07

DOI

10.1021/acs.macromol.6c00686

Universal Relationship between Limiting Current and Electrochemical Transport Properties in Malonate-Based Polymer Electrolytes

Rounak Jana [b], Lily A. Gido [a,b], Vivaan Patel [a,b], Emily E. Abdo [a,b], Shreya Makkar [a,b], Michael S. Bowen [a,b] and Nitash P. Balsara [a,b]*

[a] Department of Chemical and Biomolecular Engineering, University of California, Berkeley, CA 94720, USA

[b] Materials Sciences Division, Lawrence Berkeley National Laboratory, Berkeley, CA 94720, USA

[*]Corresponding author's email address: nbalsara@berkeley.edu

Abstract:

There is considerable interest in developing high-performance electrolytes for rechargeable lithium batteries. For practical applications, the electrolyte must support large dc currents. However, the parameters most often reported in the literature, conductivity, κ, and current fraction, $\rho_{+¿¿}$, reflect ion transport in the limit of infinitesimal currents. In this limit, the efficacy of an electrolyte is given by the product, $\kappa\rho_{+¿¿}$. The limiting current density, $i_{\lim ¿¿}$, is the maximum current density that can be applied across an electrolyte; the cell voltage diverges if the applied current density exceeds $i_{\lim ¿¿}$. This parameter reflects ion transport in the limit of large dc currents and therefore of practical interest. It would therefore be convenient if $i_{\lim ¿¿}$ could be predicted from measurements of $\kappa\rho_{+¿¿}$. In order to explore this possibility, we studied six malonate-based polymers and PEO at a fixed salt concentration ($r = 0.08$) and temperature ($90℃$) using symmetric cells with planar electrodes. Unfortunately, there is no correlation between $i_{\lim ¿¿}$ and $\kappa\rho_{+¿¿}$. When the applied current density, i is less than $i_{\lim ¿¿}$, the cell voltage approaches a stable plateau, $\phi_{plateau}$. We found a linear dependance between i and thickness-normalized plateau potential, $\phi_{plateau}L^{-1}$, irrespective of the magnitude of the applied current. In all seven polymer electrolytes, we found a linear correlation between $i_{\lim ¿¿}$ and the slopes of these lines, σ. In other words, measurements of σ can be used to predict the limiting current.

For Table of Contents Use Only

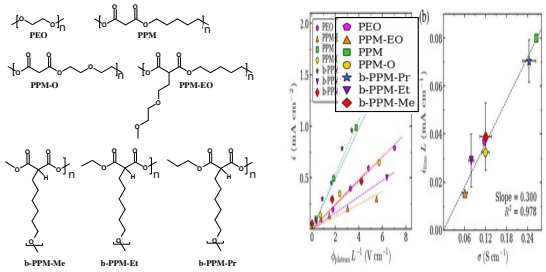

Introduction:

The electrolytes used in lithium-ion batteries are mixtures of organic liquid solvents and salt.[1] There is considerable interest in replacing the liquid solvents with polymers.[2–4] Polymer electrolytes have the potential to increase the energy density of rechargeable batteries due to their stability against lithium metal anodes.[5,6,7] It is also possible that the low flammability of the polymers may improve safety, and electrolyte degradation during charge-discharge cycles may slow down due to lower molecular mobility.[8,9]

For practical applications, electrolytes must support large currents. The limiting current density, $i_{\lim ¿¿}$, is the maximum current density that can be applied across an electrolyte; the cell voltage diverges if the applied current density exceeds $i_{\lim ¿¿}$.[10–13] Salt concentration gradients develop when current passes through an electrolyte, leading to high concentration near the positive electrode and low concentration near the negative electrode. At the limiting current, the concentration at the negative electrode approaches zero, and the cell voltage diverges.[11] In dilute electrolytes, the salt chemical potential is given by the Nernst equation, $\mu_s = \mathrm{RT}\ln c$, where c is the molar concentration. The voltage divergence at the limiting current is due to the divergence of the $\ln c$ term near the negative electrode as $c \to 0$. The limiting current is difficult to measure because many other modes of cell failure may occur, depending on the nature of the electrode-electrolyte interface. For example, cells with lithium metal electrodes fail due to the growth of dendrites on the surface of the electrodes.[14] It is therefore not surprising that there are relatively few reports of limiting current measurements in the literature despite the fact that hundreds of chemically distinct

polymer electrolytes have been studied in the literature.[15–18] It is also not surprising that the relationship between molecular structure and limiting current has not yet been established.

Ionic conductivity, κ, has been determined in virtually all the polymer electrolytes proposed in the literature. This parameter is measured by ac impedance using cells with blocking electrodes. Another popular transport parameter is current fraction, $\rho_{+¿¿}$. This parameter is measured in constant voltage experiments using cells with nonblocking electrodes, and $\rho_{+¿¿}$is defined as the ratio of the final and initial currents. In the limit of $c \to 0$, $\rho_{+¿¿}$ approaches the cation transference number as first noted by Bruce and Vincent.[19,20] Under small applied potentials, the steady-state current obtained through a symmetric lithium–electrolyte–lithium cell at a given potential is proportional to the product $\kappa\rho_{+¿¿}$.[21,22] The product $\kappa\rho_{+¿¿}$ is thus defined as the efficacy of the electrolyte at small applied potentials.

Newman's concentrated solution theory provides a rigorous framework for predicting limiting current. However, applying this theory requires knowledge of five concentration-dependent thermodynamic and transport parameters. In addition to κ, we need to determine the diffusion coefficient, D, the cation transference number with respect to solvent velocity, $t_{+¿^0¿}$, the thermodynamic factor, T_f, and the partial molar volume of salt, $\overline{V}_e$.[23] Measuring these parameters over wide concentration window is tedious and seldom done. It would therefore be convenient if the limiting current could be predicted using a single parameter like $\kappa\rho_{+¿¿}$. In other words, is the current obtained in an electrolyte under large applied potentials correlated to the efficacy at small applied potentials?

We answer this question using five newly developed malonate-based polymers. Measurement of limiting current over a wide range of salt concentrations have only been conducted on two polymers, poly(ethylene oxide) (**PEO**), and poly(pentyl malonate) (**PPM**).[24–26] Our decision to use malonate-based polymers in this study was because the limiting current of PPM is higher than that of PEO.[24] However, κ of PEO is higher than that of PPM, while $\rho_{+¿¿}$of PPM is higher than that of PEO.[26] These differences arise due to differences in the solvation structures that surround the lithium ions. In the case of PEO, lithium ions are solvated by polymer segments arranged in a crown-ether-like configuration. All the segments are donated by a single polymer chain. In the case of PPM, the lithium ions are solvated by less well-defined structures formed by two or three polymer chains.[27] This solvation structure thus results in the formation of temporary crosslinks. The addition of salt leads to an increase in the glass transition temperature (T_g) which is more pronounced in the case of PPM.[28] This accounts for the conductivity difference between PPM and PEO. The low values of $\rho_{+¿¿}$in PEO arise primarily due to field-induced motion of the solvated polymer segments. This motion is less in PPM because the solvation shell comprises more than one polymer chain.[28]

Figure 1 shows the chemical structures of the polymers used in this study. Electrolytes were made by mixing lithium bis(trifluoromethanesulfonyl)imide (LiTFSI) with the polymers. **PPM-O**, is a linear polymer with an ethylene oxide segment incorporated into the main chain. Our objective was to improve the conductivity of PPM by incorporating an EO segment in the main chain. The repeating unit of PPM-O has an extra oxygen atom relative to PPM. **PPM-EO**, incorporates a pendant side chain comprising two EO moieties emanating from the PPM backbone.

Our objective was to determine if the relationship between large and small voltage behavior is affected by the location of the EO moiety (main chain versus side chain).

The remaining three materials in Figure 1 are hyperbranched derivatives of PPM. Hyperbranched polymers possess a highly branched, three-dimensional architecture, which imparts unique properties compared to their linear analogs, resulting from increased free volume. This increase suppresses crystallinity and lowers T_g. A key property of these systems is the presence of a large concentration of end groups; the concentration of end groups in high molecular weight linear polymers is generally negligible. Recent studies have explored a variety of

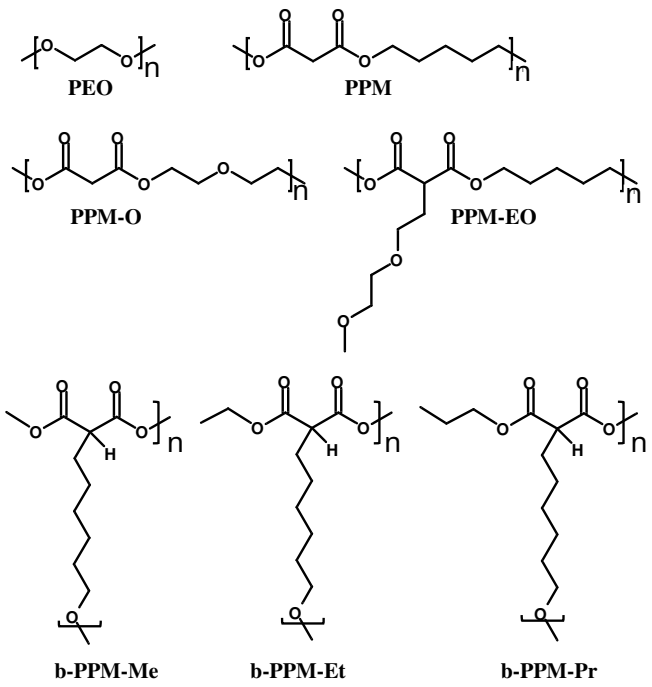

hyperbranched polymer electrolytes based on polyethers, polyesters, and polyurethanes.[29–31] In this work, we present data from three hyperbranched PPM derivatives that differ solely in their end groups—methyl, ethyl, or propyl (**b-PPM-Me, b-PPM-Et, b-PPM-Pr**).

Figure 1. Chemical structure of the polymers used in this work.

We present measurements of κ, $\rho_{+¿¿}$, and $i_{\lim ¿¿}$for the seven polymer electrolytes given in Figure 1. Our first objective was to determine the correlation between $i_{\lim ¿¿}$ and $\kappa\rho_{+¿¿}$. We find no correlation between these quantities. We did, however, find a significant correlation between $i_{\lim ¿¿}$ and a new parameter that we introduce below. We also report the values of $\phi_{\lim ¿¿}$, the potential drop necessary to obtain the limiting current. While $i_{\lim ¿¿}$varies by an order of magnitude for the electrolytes given in Figure 1, $\phi_{\lim ¿¿}$ is a constant, independent of polymer structure.

Experimental section:

Materials

Dimethyl malonate, diethyl malonate, and dipropyl malonate, 1,5-pentanediol, 6-bromo-1-hexanol, diethylene glycol, diethylene glycol monomethyl ether, pyridinium p-toluenesulfonate (PPTS), p-toluenesulfonyl chloride, and 3,4 dihydropyran were purchased from Millipore Sigma and used as received. Dry tetrahydrofuran (THF) and ethanol were also purchased from Millipore Sigma and used as received. Because titanium isopropoxide $(TiO^iPr)_4$, and sodium hydride (NaH) are air-sensitive, they were stored in an argon glovebox after they were purchased from Millipore Sigma.

Synthesis of Polymer and Characterization

Poly(pentylmalonate) (PPM) and poly(methyl (2-propoxyethyl) malonate) (PPM-O) were synthesized by direct melt condensation polymerization of dimethyl malonate with 1,5-pentanediol and diethylene glycol, respectively, at 120°C, as shown in **Scheme 1**. The reaction was catalyzed by adding a few drops of titanium isopropoxide ($Ti(O^iPr)_4$) to the reaction mixture. Polymerization

was driven toward product formation by removing the condensate (methanol) under controlled vacuum. The final polymers were purified by reprecipitating them two times from methanol and diethyl ether.

Preparation of PPM-EO was performed in two steps, as shown in Scheme 1. In the first step, excess dimethyl malonate was reacted with sodium hydride to form the monosodium salt. The monosodium salt was then reacted with diethylene glycol monomethyl ether tosylate to yield the diester monomer, dimethyl 2-(2-(2-methoxyethoxy)ethyl)malonate (compound 5). Excess unreacted dimethyl malonate was removed by distillation under 1 mm Hg vacuum at 65°C. In the final step, this diester monomer was polymerized with 1,5-pentanediol under similar polymerization conditions as mentioned above.

The synthesis of the branched polymers is described in Scheme 1. In the first step, the hydroxyl group of 6-bromohexanol was reacted with 3,4 dihydropyran to protect the hydroxyl group. In parallel, excess dimethyl malonate was reacted with sodium hydride to form the monosodium salt. The protected bromo-compound (tetrahydropyranyl (THP) ether-protected 6-bromohexanol) was reacted with the monosodium salt to yield dialkyl 2-(6-((tetrahydro-2H-pyran-2-yl)oxy)hexyl) malonate (compound 3). Excess unreacted dimethyl malonate was distilled out under 1 mm Hg vacuum at 65°C. In the next step, the THP protecting group in compound 3 was removed by refluxing in ethanol in the presence of pyridinium p-toluenesulfonate (PPTS) to obtain dialkyl 2-(6-hydroxyhexyl) malonate (compound 4). Finally, melt self-condensation polymerization was performed on compound 4 under similar conditions as described earlier.

The molecular weights of these polymers and their corresponding polydispersity index (PDI), determined by GPC, are given in Table 1.

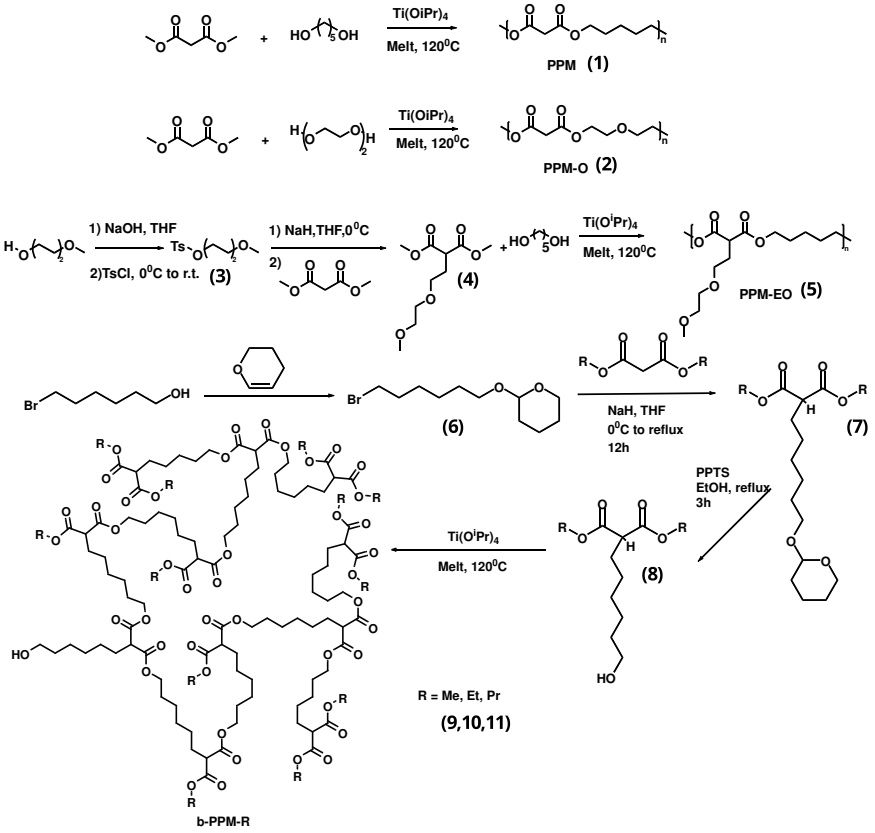

Scheme 1. Synthesis of linear and hyperbranched malonate-based polymers

Preparation of electrolytes

Electrolytes were prepared by mixing each polymer with lithium bis(trifluoromethanesulfonyl) imide (LiTFSI) salt. Due to the hygroscopic nature of LiTFSI, all sample preparation was carried out in an argon glovebox (MBraun) where H_2O and O_2 levels were maintained below 0.1 ppm and 1 ppm respectively. The set of six polyesters were dried, along with 5 kg/mol PEO (Polymer Source), at 90°C under vacuum in the glovebox antechamber for a minimum of 8 h and then transferred into the glovebox. Dry polymer and LiTFSI salt (Novolyte)

were dissolved into anhydrous tetrahydrofuran (THF) and the solutions were mixed at 60°C for 30 min. Once the solutes were fully dissolved, the caps were removed from the vials, allowing THF to evaporate and leave behind a homogeneous polymer/salt mixture. After drying on the hotplate at 90°C for 1 day, the electrolytes were transferred to the glovebox antechamber and dried under vacuum for 48 h at 125°C to remove any excess THF. The dry electrolytes were very viscous liquids at room temperature with the consistency of molasses.

Differential scanning calorimetry

Samples were prepared by depositing 3–7 mg of each electrolyte into hermetically sealed aluminum pans. Differential scanning calorimetry (DSC) experiments were performed on a TA Instruments DSC Q200 instrument with the following temperature scan: heat to 150°C at 10°C/min, cool to −75°C at 5°C/min, heat to 150 °C at 10°C/min. The glass transition temperature, T_g, values of the electrolytes were obtained from the second heating scan. T_g measurements were found to be repeatable within 1°C.

Experimental information for electrochemical measurements

All electrochemical cells were prepared within an argon glovebox with oxygen and water concentrations below 1 ppm. Stainless-steel symmetric cells were used to measure the conductivity, κ, of our electrolytes. These cells were constructed by filling silicone spacer material (McMaster Carr) (internal diameter of 3.175 mm and thickness of 500 μm) with our electrolytes and sandwiching them between two 200 μm thick stainless-steel electrodes. The thickness of the stack was measured with a micrometer to find the final electrolyte thickness, L. Nickel tabs (MTI

Corp.) were attached to the electrodes, and the cells were vacuum sealed in laminated pouch material (MTI Corp).

Conductivity measurements were made using stainless-symmetric cells. The cells were annealed at 90ºC for at least 3 hours before experiments were performed. Conductivity measurements were made at various temperatures from 30 to 90ºC using electrochemical impedance spectroscopy (EIS). Measurements were made by applying a sinusoidal voltage profile with an amplitude of 40 mV and frequencies ranging from 1 MHz to 1 Hz to identify the bulk impedance, R_b. The conductivity was then calculated using,

$$\kappa = \frac{L}{A R_b}, \quad (1)$$

where A is the electrochemically active area, and L is the electrolyte thickness.

Lithium (MTI Corp.) symmetric cells were used for measurements of the salt diffusion coefficient, D, and current fraction, $\rho_{+¿¿}$. These cells were constructed similarly to the stainless-steel symmetric cells. Lithium metal electrode was brushed and pressed using a pneumatic press, then the thickness was measured using a micrometer. The silicone spacer material (McMaster Carr) (internal diameter of 3.175 mm) was placed on one metal electrode, and the electrolyte was loaded into the cell. The second lithium metal electrode was placed in contact with the electrolyte and stainless-steel shims were placed on top of each lithium metal electrode. The thickness of the stack was measured with a micrometer, and the electrolyte thickness was calculated by subtracting the thickness of the electrodes and stainless-steel shims from the total thickness. Nickel tabs were then attached to the stainless-steel discs, and the stack was vacuum sealed in laminated pouch material.

The current fraction was measured using lithium symmetric cells following previously described methods.[19,24,26] All measurements with lithium symmetric cells were performed at 90ºC. Cells were annealed at 90ºC for at least three hours and preconditioned for 4 cycles where a single cycle consists of one 2 h polarization of 3 μA, a 4 h relaxation at open circuit voltage (OCV), a 2 h polarization at -3 μA, and another 4 h relaxation step. The resistance of the electrolyte was measured during preconditioning to track changes in the bulk and interfacial impedance, R_i and to ensure the formation of a stable solid electrolyte interface (SEI). After preconditioning, a potential was applied to the cell until the measured current reached a steady state value, i_{ss}. During this polarization, impedance measurements were made to track R_b and R_i. A modified version of the equation developed by Bruce and Vincent was used to calculate the current fraction:

$$\rho_{+} \frac{i_{ss}\left(\Delta V - i_{\Omega} R_{i,0}\right)}{i_{\Omega}\left(\Delta V - i_{SS} R_{i,SS}\right)}, \quad (2)$$

$i_{\Omega}$is the calculated initial current, ($i_{\Omega}=\frac{\Delta V}{R_{i,0}+R_{b,0}}$), where subscripts 0 and ss indicate the initial and steady state values respectively. For these experiments ΔV values of ±10 was used. After polarization, the cells were allowed to relax, and the resulting decline in potential was fit to an exponential equation,

$$V(t)=k_0+k_1 e^{-k_2 t}, \quad (3)$$

where k_0 is the fitted offset voltage and k_1 and k_2 are fit parameters. The salt diffusion coefficient was calculated using equation 4 as described in reference 26. [26]

$$D = \frac{L^2 k_2}{\pi^2}, \quad (4)$$

All parameters reported here represent averages of three independent measurements and the standard deviation was used as the error bar. Parameters for PEO and PPM were taken from reference 32,[32] and 26.[26]

Limiting current density measurements

Lithium-lithium symmetric cells were used for measurements of $i_{\lim ¿¿}$ of b-PPM-Me, b-PPM-Et, and b-PPM-Pr.[24] Lithium-indium alloy electrodes[11] were used to determine $i_{\lim ¿¿}$ of PEO, PPM, PPM-O, and PPM-EO as these electrolytes were not stable against lithium metals. The atomic fraction of lithium in the lithium-indium electrodes was 0.4. In one case, b-PPM-Et, both kinds of cells were examined to ensure consistency. The cells were constructed and preconditioned as described in ref 6. An initial impedance measurement was taken, followed by constant current polarization. After a stable plateau in the potential was reached, or the potential diverged, the cell was allowed to relax at open circuit, and then a final impedance measurement was taken. The limiting current density was determined by systematically increasing the applied current density and noting the nature of the cell potential vs time data. More details are given in the results and discussion section.

Results and discussion:

Electrochemical properties of an electrolyte depend on the ratio of polar groups to Li^+ ions. We define *r* as the ratio of oxygen atoms in a polymer to Li^+ ions. In our previous studies on PPM, we obtained the highest limiting current at $r = 0.08$.[24] Therefore, we kept *r* fixed at this value for all the polymers shown in Figure 1. For simplicity, we refer to electrolytes using just name of the polymer. The physical properties of the electrolytes are summarized in Table 1.

Table 1. Physical Characterization of the electrolytes with r = 0.08.

Sample	Mn* (kDa)	PDI*	T_g# (°C)	κ (S/cm) $	$\rho_{+¿¿}$ $	D (cm/s) $
PEO	5.0	1.05	-23	$(9\pm0.1)\times10^{-4}$	0.07 ± 0.001	$(6.8\pm0.1)\times10^{-8}$
PPM	7.32	1.32	-18	$(6\pm0.1)\times10^{-4}$	0.57 ± 0.03	$(1.1\pm0.1)\times10^{-7}$
PPM-O	4.58	1.26	-5	$(2.9\pm0.55)\times10^{-4}$	0.62 ± 0.057	$(1.8\pm0.9)\times10^{-7}$
PPM-EO	8.12	4.04	-27	$(8.4\pm0.37)\times10^{-4}$	0.24 ± 0.011	$(2.4\pm0.2)\times10^{-7}$
b-PPM-Me	-	-	-46	$(1.3\pm0.46)\times10^{-4}$	0.3 ± 0.009	$(1.2\pm1.3)\times10^{-7}$
b-PPM-Et	17.33	5.12	-21	$(1.2\pm0.22)\times10^{-4}$	0.39 ± 0.03	$(1.2\pm0.8)\times10^{-7}$
b-PPM-Pr	25.04	5.76	-28	$(1.1\pm0.31)\times10^{-4}$	0.55 ± 0.046	$(1.6\pm0.4)\times10^{-7}$

*** Measured from GPC traces in THF as eluent in three detector system**

 # Measured using DSC

$ Measurements were done at 90°C

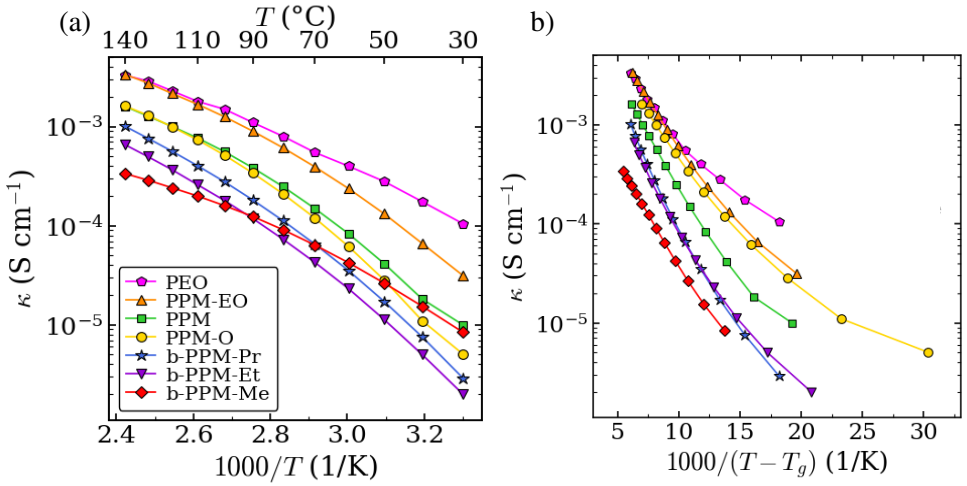

Figure 2. Temperature dependence of conductivity, κ, of all seven electrolytes (r = 0.08) from 30 to 140°C (a) κ vs 1000/T. The conductivities of all PPM-based electrolytes were lower than that PEO at all temperature range. (b) κ vs 1000/(T-T_g), where the glass transition temperature, T_g, is determined by Differential Scanning Calorimetry (DSC) and reported in the Supplemental Information (Figure S13).

Conductivity (κ) was measured across a temperature range of 30–140°C for each polymer. Figure 2a shows logκ plotted against 1000/T. PEO exhibits the highest conductivity. Interestingly,

at temperatures above 110°C, PPM-EO and PEO have comparable conductivities. PPM and PPM-O exhibit intermediate values of conductivities followed by the hyperbranched electrolytes. The

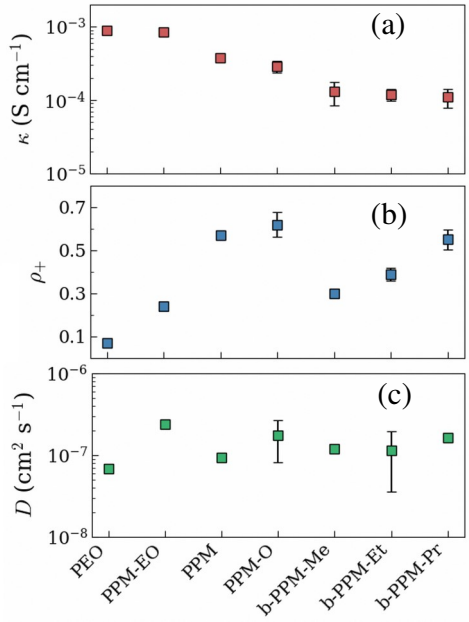

Figure 3. Electrochemical characterization of the electrolytes (r = 0.08 at 90°C). (a) conductivity, κ, (b) current fraction, $\rho_{+¿¿}$, and (c) diffusion coefficient, D. An inverse relationship is observed between κ and $\rho_{+¿¿}$. For the branched polymers, the conductivities are similar but $\rho_{+¿¿}$ increases with increasing end group length. D is independent of the molecular structure of the polymer.

behavior of b-PPM-Pr and b-PPM-Et is surprisingly similar to that of the linear polymer. The only outlier is b-PPM-Me which has a shallower temperature dependence than the others. Figure 2b shows logκ plotted against 1000/(T-T_g). The measurement of T_g is described in the Supplemental Information (Figure S13). If conductivity were governed entirely by segmental motion, then the data shown in Figure 2b would have collapsed on to a single curve. It is perhaps surprising that the spread of the data in Figures 2a and 2b are comparable. This suggests that conductivity of different malonate-based electrolytes is not coupled to segmental motion to the same extent.

In the remainder of the paper, we focus on the data obtained at 90°C. Figure 3 presents the κ, D, and $\rho_{+¿¿}$ of these polymer electrolytes at 90°C. A clear trend emerges among the linear

polymer electrolytes: polymers with high κ exhibit low $\rho_{+¿¿}$. This trend has been noted in prior

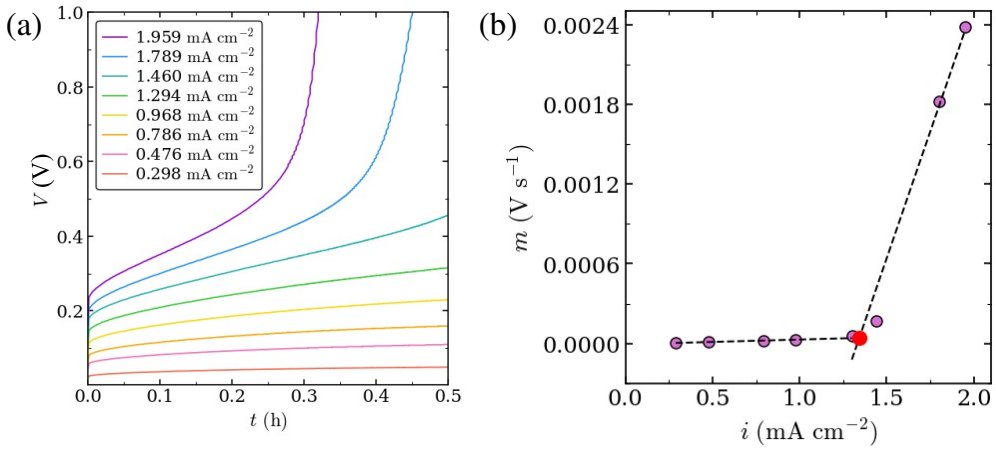

publications.[18,33] The conductivities of the branched electrolytes are similar but $\rho_{+¿¿}$increases with increasing end group length. This enhancement in $\rho_{+¿¿}$ without a corresponding penalty in κ is unusual. $\rho_{+¿¿}$ of b-PPM-Pr is comparable to the linear polymer with highest $\rho_{+¿¿}$, PPM-O. To a good approximation, D is independent of the molecular structure of the polymer.

Figure 4. Representative example of limiting current determination in a constant current experiment. (a) Time-dependence of potential (V) in a lithium–lithium symmetric cell with a b-PPM-Pr/LiTFSI electrolyte at r = 0.08 and 90°C, at various applied current densities. At low current densities, the potential reaches a steady-state plateau; however, above a threshold current density the potential diverges toward the cut-off voltage of 1V. (b) The last 20% of the data obtained in (a) at each current density were fit to a straight line and the slope of this line, m, is plotted as a function of current density. The data in this plot were to fit to two lines following reference 32. The intersection of these lines is taken as $i_{\mathrm{lim}\,¿¿}$.

We now discuss the limiting current measurements. Figure 4a shows the time-dependence of potential, V of b-PPM-Pr at various applied current densities, i. The interfacial contribution is deducted from the measured potential, V according to equation 5.

$$\phi = V - R_i\, i \quad (5)$$

At low current densities, the potential, ϕ reaches a steady-state plateau, $\phi_{plateau}$; however, above a threshold current density the potential diverges toward the cut-off voltage of 1V. The last 20% of the data obtained were fit to a straight line and the slope of this line, m, is plotted as a function of current density in Figure 4b. The data in this plot were to fit to two lines following reference 34. [34] The intersections of these lines are taken as $i_{\lim}$¿¿.

To accurately determine the limiting current, our analysis focuses on the time dependence of ϕ/L during the final 20% of the experiment (Δt). When the applied current exceeds the limiting current density in a binary electrolyte, the potential increases sharply toward the end of the measurement. In contrast, when the current is below the limiting value, the potential asymptotically approaches a time-independent plateau, $\phi_{plateau}$. This distinction becomes clear when the long-time response is examined, and the limiting current is identified as the inflection point in the ϕ/L versus Δt plot. A representative analysis is shown in Figure 4b.

All linear polymers, including PPM and PEO, were unstable against lithium metal at high

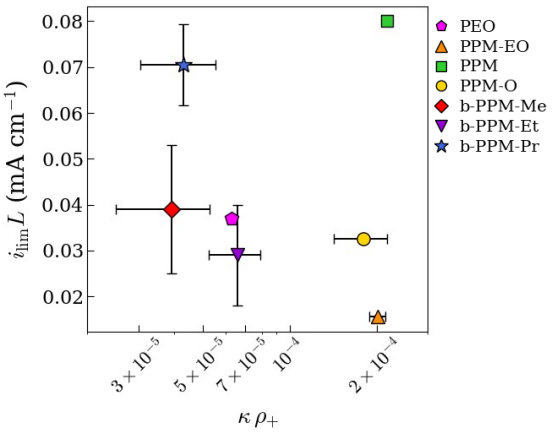

applied current densities; as reported in earlier studies,[11,35] cells failed due to lithium dendrite

formation. Symmetric cells with lithium-indium electrodes were used to determine the limiting current in these systems. In contrast, the hyperbranched PPMs (all three variants) exhibited dendrite-resistant behavior under the same conditions. This enabled the measurement of limiting currents in symmetric cells with lithium electrodes. In one hyperbranched PPM (b-PPM-Et), we measured limiting current using two kinds of cells, one with lithium-indium electrodes and other with lithium electrodes (Figure S16). Results obtained from both kinds of cells were within experimental error.

Figure 5. Plot of thickness-normalized limiting current, $i_{\mathrm{lim}}L$, against efficacy, $\kappa\rho_{+}$of all seven electrolytes (r = 0.08) at 90°C. No correlation between $i_{\mathrm{lim}}L$ and efficacy, $\kappa\rho_{+}$ is observed.

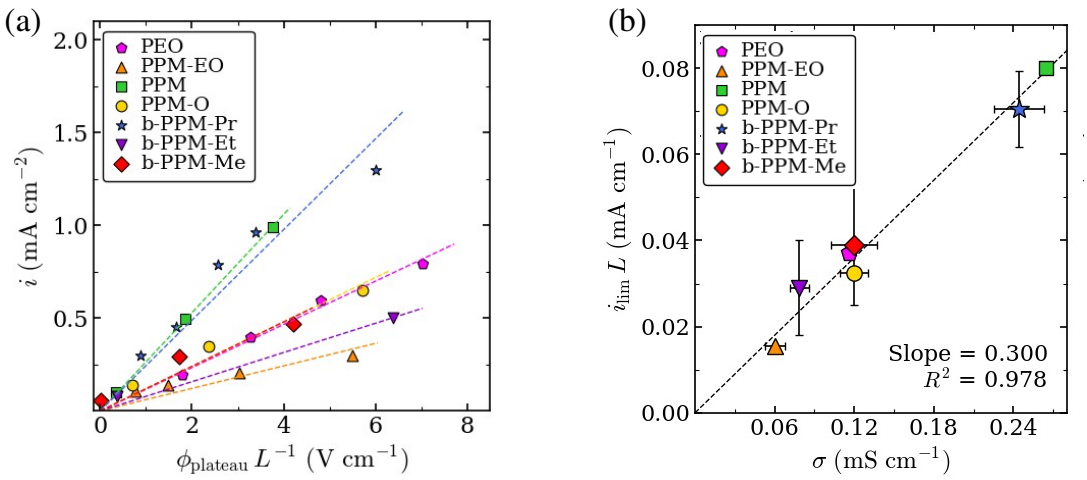

The parameter $i_{\mathrm{lim}}L$ quantifies ion transport under large applied potentials, while $\kappa\rho_{+}$ quantifies ion transport under small applied potentials. $\kappa\rho_{+}$ is much easier to measure than $i_{\mathrm{lim}}L$, but $i_{\mathrm{lim}}L$ is important for practical applications. We therefore investigated whether these two parameters were correlated with each other. Figure 5 shows a plot of thickness-normalized limiting current, $i_{\mathrm{lim}}L$, versus efficacy, $\kappa\rho_{+}$. This figure shows that $\kappa\rho_{+}$ and $i_{\mathrm{lim}}L$ are not correlated with each other. For instance, the $\kappa\rho_{+}$value of PPM-O is nearly identical to that of

PPM, yet the limiting current of PPM-O is approximately 1.5 times lower. These results indicate that the limiting current ($i_{\lim ¿¿}$) is governed by a complex interplay between five concentration-dependent parameters κ, D, $t_{+¿^{0}¿}$, T_f, and $\overline{V_e}$.

Figure 6. (a) A plot of current density, i, versus thickness-normalized plateau potential, $\phi_{plateau}\ L^{-1}$ in symmetric cells with seven different electrolytes as indicated in the legend. The salt concentration and the temperature are held fixed ($r = 0.08$ and 90°C). The lines represent least squared fits through the data constrained to pass through the origin. We define σ to be equal to the slopes of these lines. (b) Thickness-normalized limiting current, $i_{\lim ¿¿}L$, versus σ. To a good approximation, $i_{\lim ¿¿}L$ is a linear function of σ.

When the applied current density, i is lower than the limiting current, a stable potential is obtained. We refer to this stable potential as $\phi_{plateau}$. In the example shown in Figure 4, we were able to determine $\phi_{plateau}$ at the four lowest values of i. This was repeated for all datasets to obtain the dependence of thickness-normalized stable potentials ($\phi_{plateau}/L$) on i. The results are shown in Figure 6a where $\phi_{plateau}/L$ is plotted as a function of i for all electrolytes. To a good approximation, the data obtained from each electrolyte fall on a straight line. The lines in Figure 6a represent least squares fit through the origin. We define σ to be equal to the slopes of these lines. In Figure 6b we plot $i_{\lim ¿¿}L$ versus σ. It is evident that there is an excellent correlation between the two parameters. To a good approximation, $i_{\lim ¿¿}L$ is a linear function of σ. This indicates that σ is a much better descriptor of ion transport under large applied currents than $\kappa\rho_{+¿¿}$. Among the seven electrolytes studied, PPM and b-PPM-Pr exhibit the highest σ values and also the highest $i_{\lim ¿¿}L$ values, placing them in the top-right corner of the σ– $i_{\lim ¿¿}L$ plot. $i_{\lim ¿¿}L$ of PPM and b-PPM-Pr are 0.08 and 0.07 mA/cm. Conversely, PPM-EO, which has the smallest limiting current (0.016 mA/cm), exhibits

the smallest σ. PEO, b-PPM-Me, and PPM-O fall in the intermediate region with thickness-normalized limiting currents between 0.03 mA/cm and 0.04 mA/cm. The straight line in Figure 6b represents

$$\frac{i_{\lim ¿ L}}{\sigma} = 0.3 V ¿ \quad (6)$$

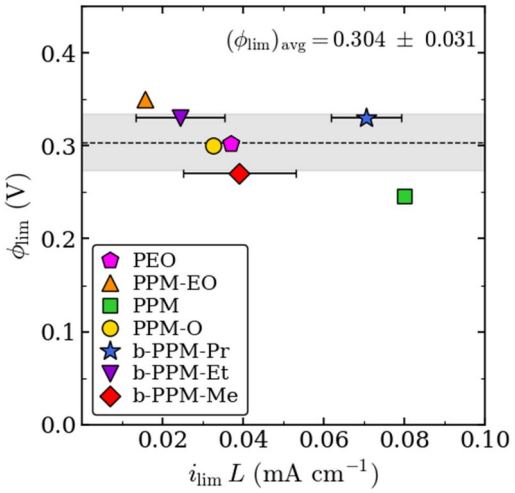

Figure 7. Plot of limiting potential, $\phi_{\lim ¿¿}$ versus thickness normalized limiting current, $i_{\lim ¿¿} L$ for all seven electrolytes at r = 0.08 at 90°C. $\phi_{\lim ¿¿}$ for all the electrolytes is 0.304 ± 0.031 V, independent of their limiting current values.

When the current density exceeds the limiting current, the cell voltage diverges. We, therefore, define the limiting potential, $\phi_{\lim ¿¿}$ as the voltage drop that corresponds to the highest current density that gave a stable cell voltage at long times. Experimentally, $\phi_{\lim ¿¿}$ is obtained by subtracting the interfacial impedance contribution from the measured steady potential:[21]

$$\phi_{\lim ¿}=V_{\lim ¿}-R_{¿}\, i_{\lim ¿}. \quad (7)$$

In Figure 7, we plot the potential drops ($\phi_{\lim ¿¿}$) as a function of the thickness-normalized limiting current densities ($i_{\lim ¿¿}L$) for all seven electrolytes. We observe that $\phi_{\lim ¿¿}$ remains essentially constant across all electrolytes:

$$\phi_{\lim ¿=0¿}.304 \pm 0.031 \text{ V}. \quad (8)$$

Equations 6 and 8 are equivalent. The constant perfector on the right side of equation 6 is identical to the right side of equation 8. These equations indicate that a master plot can be obtained if $i/i_{\lim ¿¿}$is plotted versus $\phi_{plateau}/\phi_{\lim ¿¿}$. This plot, which encompasses all seven electrolytes, is shown in Figure 8. The data from all seven electrolytes collapse on to a master line as expected. The collapse is far from perfect. Some systems like PPM-EO lie above the line, while others like PPM lie below the line. We do not have any explanation for this observation.

The reason for the behaviors seen in Figures 6 through 8 remains to be established. Ultimately one would need to determine the underlying transport and thermodynamic parameters. At the limiting current, the salt concentration at the negative electrode is zero, and that at the positive electrode is about 2r. In other words, the concentration profiles obtained in all electrolytes are similar at limiting current. Perhaps, the observation that $\phi_{\lim ¿¿}$ is independent of chemical identity is related to this similarity.

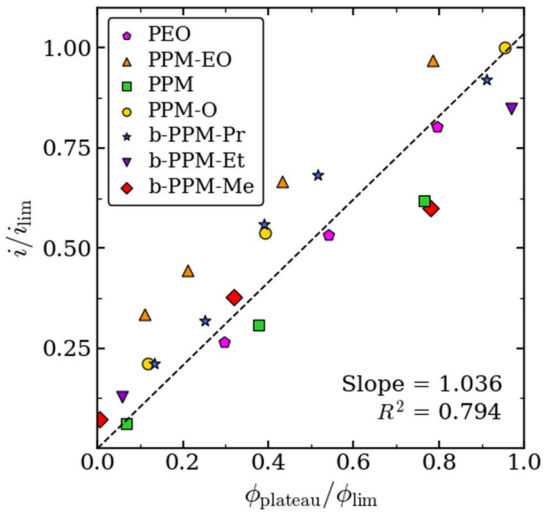

Figure 8. Master plot describing current-voltage relationships of all seven electrolytes at $r = 0.08$ at 90°C. The ratio of the applied current densities and the limiting currents, $i/i_{\lim ¿¿}$ are plotted against the ratio of plateau potentials and the limiting potentials, $\phi_{plateau}/\phi_{\lim ¿¿}$. The line represents a least-squared fit through the data constrained to pass through the origin. To a good approximation, the slope of the line is equal to 1.

Conclusions:

The limiting current, $i_{\lim ¿¿}$ of an electrolyte is of primary importance for practical applications. Another important parameter is the voltage drop needed to obtain the limiting current; we call this quantity limiting voltage, $\phi_{\lim ¿¿}$. Limiting current and limiting voltage can be predicted using Newman's concentrated solution theory, but this requires performing arduous experiments to determine five concentration-dependent transport and thermodynamic parameters. Of these parameters, only conductivity, κ, and current fraction, $\rho_{+¿¿}$, are widely reported in the literature, and the efficacy of an electrolyte in the limit of small applied potentials is the product, $\kappa\rho_{+¿¿}$. It would therefore be convenient if there were a correlation between $i_{\lim ¿¿}$and $\kappa\rho_{+¿¿}$. In order to explore this, we studied six malonate-based polymers and PEO at a fixed salt concentration (r = 0.08) and temperature (90℃). Within this set of the polymer electrolytes, the limiting currents of PPM and b-PPM-Pr are significantly higher than those of other electrolytes. In these seven polymer electrolytes, however, there is no correlation between $i_{\lim ¿¿}$ and $\kappa\rho_{+¿¿}$.

The standard protocol for determining $i_{\lim ¿¿}$ is to measure the time-dependent voltage of a symmetric cell containing the electrolyte of interest at a fixed applied current density, i. When i is less than $i_{\lim ¿¿}$ the cell voltage approaches a stable plateau, $\phi_{plateau}$. To a good approximation, we found a linear dependance between i and $\phi_{plateau}$ L^{-1} in this regime. In all seven polymer electrolytes, we found a linear correlation between $i_{\lim ¿¿}$ and the slopes of these lines, σ (equation 6). In other words, measurements of σ can be used to predict the limiting current. A direct consequence of the linear dependence of $i_{\lim ¿¿}$ and σ is that $\phi_{\lim ¿¿}$ is constant. Our work thus far is limited to a fixed salt concentration and temperature. Studying the relationship between i and $\phi_{plateau}$ at other salt concentrations and temperatures seem warranted.

Supporting Information. Experimental details of synthesis and characterization; NMR spectra of intermediates, monomers, polymers; experimental details of electrolyte preparation, electrochemical characterization and GPC, DSC spectra, dependence of limiting current with conductivity and current fraction, comparison of the limiting current density determined using Li/Li symmetric cells and Li/In (40 atom % Li) symmetric cells.

Acknowledgement

This work was primarily supported by the Assistant Secretary for Energy Efficiency and Renewable Energy, Office of Vehicle Technologies, of the U.S. Department of Energy, under Contract DE-AC02-05CH11231 under the Battery Materials Research Program. Work at the Molecular Foundry was supported by the Office of Science, Office of Basic Energy Sciences, of the U.S. Department of Energy under Contract No. DE-AC02-05CH11231, under proposal number MFP- 10100.

References

(1) Xu, K. Li-Ion Battery Electrolytes. *Nat. Energy* **2021**, *6* (7), 763. https://doi.org/10.1038/s41560-021-00841-6.

(2) Paren, B. A.; Häußler, M.; Rathenow, P.; Mecking, S.; Winey, K. I. Decoupled Cation Transport within Layered Assemblies in Sulfonated and Crystalline Telechelic Polyethylenes. *Macromolecules* **2022**, *55* (7), 2813–2820. https://doi.org/10.1021/acs.macromol.2c00132.

(3) Jang, S.; Tsai, R. Bin; Schroeder, C. M.; Evans, C. M. Anion and Cation Size Effects on Viscoelasticity and Ion Transport of Imine Vitrimer Electrolytes. *Chemistry of Materials* **2025**, *37* (18), 7037–7048. https://doi.org/10.1021/acs.chemmater.5c00991.

(4) Ganesan, V.; Zhang, Z.; Marioni, N. Dynamical Ion Correlations in Polymer and Membrane Electrolytes: Recent Advances and Open Questions. *Journal of Physical Chemistry Letters*. American Chemical Society November 4, **2025**, pp 8114–8124. https://doi.org/10.1021/acs.jpclett.5c02006.

(5) Zhao, Q.; Stalin, S.; Zhao, C.-Z.; Archer, L. A. Designing Solid-State Electrolytes for Safe, Energy-Dense Batteries. *Nature Reviews Materials* **2020**, *5*, 229–252. https://doi.org/10.1038/s41578-019-0165-5.

(6) Zurita-García, L.; Wheeler, D. R. Dual-Domain Solid-State Electrolyte Made by Combining an Electrospun Skeleton with a Composite Slurry. *J. Electrochem. Soc.* **2025**, *172* (9), 090540. https://doi.org/10.1149/1945-7111/ae08f1.

(7) Rojaee, R.; Cavallo, S.; Mogurampelly, S.; Wheatle, B. K.; Yurkiv, V.; Deivanayagam, R.; Foroozan, T.; Rasul, M. G.; Sharifi-Asl, S.; Phakatkar, A. H.; Cheng, M.; Son, S. B.; Pan, Y.; Mashayek, F.; Ganesan, V.; Shahbazian-Yassar, R. Highly-Cyclable Room-Temperature

Phosphorene Polymer Electrolyte Composites for Li Metal Batteries. *Adv. Funct. Mater.* **2020**, *30* (32). https://doi.org/10.1002/adfm.201910749.

(8) Armand, M. Polymer Solid Electrolytes - an Overview. *Solid State Ion.* **1983**, *9–10* (PART 2), 745–754. https://doi.org/10.1016/0167-2738(83)90083-8.

(9) An, Y.; Han, X.; Liu, Y.; Azhar, A.; Na, J.; Kumar, N. A.; Wang, S.; Yu, J.; Yamauchi, Y. Progress in Solid Polymer Electrolytes for Lithium-Ion Batteries and Beyond. *Small* **2022**, *18* (3), 2103617. https://doi.org/10.1002/smll.202103617

(10) Selman, J. R.; Tobias, C. W. Mass-Transfer Measurements by the Limiting-Current Technique. In *Advances in Chemical Engineering*; Drew, T. B., Cokelet, G. R., Hoopes, J. W., Vermeulen, T., Eds.; Academic Press, **1978**; Vol. 10, pp 211–318. https://doi.org/https://doi.org/10.1016/S0065-2377(08)60134-9.

(11) Lee, J.; Kim, S. Y.; Hoffman, Z. J.; Chen, G.; Balsara, N. P. Experimental Platform for Determining the Maximum Limiting Current in a Polymer Electrolyte. *ACS Energy Lett.* **2024**, *9* (4), 1796–1802. https://doi.org/10.1021/acsenergylett.4c00480.

(12) Shah, D. B.; Kim, H. K.; Nguyen, H. Q.; Srinivasan, V.; Balsara, N. P. Comparing Measurements of Limiting Current of Electrolytes with Theoretical Predictions up to the Solubility Limit. *The Journal of Physical Chemistry C* **2019**, *123* (39), 23872–23881. https://doi.org/10.1021/acs.jpcc.9b07121.

(13) Selman, J. R.; Tobias, C. W. Mass-Transfer Measurements by the Limiting-Current Technique. In *Advances in Chemical Engineering*; Drew, T. B., Cokelet, G. R., Hoopes, J. W., Vermeulen, T., Eds.; Academic Press, **1978**; Vol. 10, pp 211–318. https://doi.org/https://doi.org/10.1016/S0065-2377(08)60134-9.

(14) Frenck, L.; Sethi, G. K.; Maslyn, J. A.; Balsara, N. P. Factors That Control the Formation of Dendrites and Other Morphologies on Lithium Metal Anodes. *Frontiers in Energy Research*. Frontiers Media S.A. November 1, **2019**. https://doi.org/10.3389/fenrg.2019.00115.

(15) Mindemark, J.; Imholt, L.; Brandell, D. Synthesis of High Molecular Flexibility Polycarbonates for Solid Polymer Electrolytes. *Electrochim. Acta* **2015**, *175*, 247–253. https://doi.org/10.1016/j.electacta.2015.01.074.

(16) Sun, B.; Mindemark, J.; Edström, K.; Brandell, D. Polycarbonate-Based Solid Polymer Electrolytes for Li-Ion Batteries. *Solid State Ion.* **2014**, *262*, 738–742. https://doi.org/10.1016/j.ssi.2013.08.014.

(17) Sun, B.; Mindemark, J.; Morozov, E. V.; Costa, L. T.; Bergman, M.; Johansson, P.; Fang, Y.; Furó, I.; Brandell, D. Ion Transport in Polycarbonate Based Solid Polymer Electrolytes: Experimental and Computational Investigations. *Physical Chemistry Chemical Physics* **2016**, *18* (14), 9504–9513. https://doi.org/10.1039/c6cp00757k.

(18) Rugh, H. J.; Lee, J.; Sun, C.; Abdo, E. E.; Bem, J. N.; Balsara, N. P.; Coates, G. W. Polysilaketals: High-Performance Polyether-Based Electrolytes with Tunable Disubstituted Silane Linkers. *Angewandte Chemie - International Edition* **2025**, *64* (2). https://doi.org/10.1002/anie.202415069.

(19) Watanabe, M.; Nagano, S.; Sanui, K.; Ogata, N. Estimation of Li^+ transport number in polymer electrolytes by the combination of complex impedance and potentiostatic polarization measurements; *Solid State ion,***1988**, *28-30*, 911-917.

(20) Evans, J.; Vincent, C. A.; Bruce, P. G. Electrochemical Measurement of Transference Numbers in Polymer Electrolytes, *Polymer*, **1987**, *28* (13), 2324-2328.

(21) Galluzzo, M. D.; Maslyn, J. A.; Shah, D. B.; Balsara, N. P. Ohm's Law for Ion Conduction in Lithium and beyond-Lithium Battery Electrolytes. *Journal of Chemical Physics* **2019**, *151* (2). https://doi.org/10.1063/1.5109684.

(22) Jones, S. D.; Nguyen, H.; Richardson, P. M.; Chen, Y. Q.; Wyckoff, K. E.; Hawker, C. J.; Clément, R. J.; Fredrickson, G. H.; Segalman, R. A. Design of Polymeric Zwitterionic Solid Electrolytes with Superionic Lithium Transport. *ACS Cent. Sci.* **2022**, *8* (2), 169–175. https://doi.org/10.1021/acscentsci.1c01260.

(23) Newman, J.; Thomas-Alyea, K. E. *Electrochemical Systems*; Wiley-Interscience: Hoboken, NJ, **2004**.

(24) Yu, X.; Hoffman, Z. J.; Lee, J.; Fang, C.; Gido, L. A.; Patel, V.; Eitouni, H. B.; Wang, R.; Balsara, N. P. A Practical Polymer Electrolyte for Lithium and Sodium Batteries: Poly(Pentyl Malonate). *ACS Energy Lett.* **2022**, *7* (11), 3791–3797. https://doi.org/10.1021/acsenergylett.2c02128.

(25) Lee, J.; Kim, S. Y.; Hoffman, Z. J.; Chen, G.; Balsara, N. P. Experimental Platform for Determining the Maximum Limiting Current in a Polymer Electrolyte. *ACS Energy Lett.* **2024**, *9* (4), 1796–1802. https://doi.org/10.1021/acsenergylett.4c00480.

(26) Lee, J.; Hoffman, Z. J.; Chakraborty, S.; Patel, V.; Balsara, N. P. Toward Optimization of Polymer Electrolytes by Electrochemical Characterization: Poly(Pentyl Malonate) versus Poly(Ethylene Oxide). *ACS Energy Lett.* **2025**, *10* (2), 831–836. https://doi.org/10.1021/acsenergylett.4c03525.

(27) Fang, C.; Chakraborty, S.; Li, Y.; Lee, J.; Balsara, N. P.; Wang, R. Ion Solvation Cage Structure in Polymer Electrolytes Determined by Combining X-ray Scattering and Simulations. *ACS Macro Lett.* **2023**, *12* (9), 1244–1250. https://doi.org/10.1021/acsmacrolett.3c00430.

(28) Fang, C.; Yu, X.; Chakraborty, S.; Balsara, N. P.; Wang, R. Molecular Origin of High Cation Transference in Mixtures of Poly(pentyl malonate) and Lithium Salt. *ACS Macro Lett.* **2023**, *12* (5), 612–618. https://doi.org/10.1021/acsmacrolett.3c00041.

(29) Chen, G.; Ye, L.; Zhang, K.; Gao, M.; Lu, H.; Xu, H.; Bai, Y.; Wu, C. Hyperbranched Polyether Boosting Ionic Conductivity of Polymer Electrolytes for All-Solid-State Sodium Ion Batteries. *Chemical Engineering Journal* **2020**, *394*. https://doi.org/10.1016/j.cej.2020.124885.

(30) Petry, J.; Dan, K.; Nag, A.; Thelakkat, M.; Ghosh, S. Easily Accessible Linear and Hyperbranched Polyesters as Solid Polymer Electrolytes. *Eur. Polym. J.* **2024**, *210*. https://doi.org/10.1016/j.eurpolymj.2024.112965.

(31) Wang, H.; Li, X.; Zeng, Q.; Li, Z.; Liu, Y.; Guan, J.; Jiang, Y.; Chen, L.; Cao, Y.; Li, R.; Wang, A.; Wang, Z. xiang; Zhang, L. A Novel Hyperbranched Polyurethane Solid Electrolyte for Room Temperature Ultra-Long Cycling Lithium-Ion Batteries. *Energy Storage Mater.* **2024**, *66*. https://doi.org/10.1016/j.ensm.2024.103188.

(32) Newman, J.; Chapman, T. W. Restricted Diffusion in Binary Solutions. *AIChE Journal* **1973**, *19* (2), 343–348. https://doi.org/10.1002/aic.690190220.

(33) He, Z.; Balsara, N. P. Understanding the Conductivity and Transference Trade-Off in Polymer Electrolytes Using a Robeson-Inspired Upper Bound. *ACS Appl. Polym. Mater.* **2025**, *7* (10), 5960–5968. https://doi.org/10.1021/acsapm.5c00288.

(34) Hoffman, Z. J.; Mistry, A.; Srinivasan, V.; Balsara, N. P. Comparing Experimentally-Measured Sand's Times with Concentrated Solution Theory Predictions in a Polymer Electrolyte. *J. Electrochem. Soc.* **2023**, *170* (12), 120524. https://doi.org/10.1149/1945-7111/ad1470.

(35) Grundy, L. S.; Fu, S.; Hoffman, Z. J.; Balsara, N. P. Electrochemical Characterization of PEO/LiTFSI Electrolytes Near the Solubility Limit. *Macromolecules* **2022**, *55* (20), 9030–9038. https://doi.org/10.1021/acs.macromol.2c01655.